

Synthesis of new ultrasonic-assisted palladium oxide nanoparticles: an in vitro evaluation on cytotoxicity and DNA/BSA binding properties

Ziba Sorinezami, Hassan Mansouri-Torshizi, Mohammad Aminzadeh, Arezou Ghahghaei, Nasimeh Jamgohari & Mostafa Heidari Majd

To cite this article: Ziba Sorinezami, Hassan Mansouri-Torshizi, Mohammad Aminzadeh, Arezou Ghahghaei, Nasimeh Jamgohari & Mostafa Heidari Majd (2019): Synthesis of new ultrasonic-assisted palladium oxide nanoparticles: an in vitro evaluation on cytotoxicity and DNA/BSA binding properties, Journal of Biomolecular Structure and Dynamics, DOI: [10.1080/07391102.2018.1546619](https://doi.org/10.1080/07391102.2018.1546619)

To link to this article: <https://doi.org/10.1080/07391102.2018.1546619>

 View supplementary material 

 Published online: 02 Jan 2019.

 Submit your article to this journal 

 View Crossmark data 



Synthesis of new ultrasonic-assisted palladium oxide nanoparticles: an in vitro evaluation on cytotoxicity and DNA/BSA binding properties

Ziba Sorinezami^a, Hassan Mansouri-Torshizi^b, Mohammad Aminzadeh^b, Arezou Ghahghaei^c, Nasimeh Jamgohari^b and Mostafa Heidari Majd^d

^aDepartment of Chemistry, University of Zabol, Zabol, Iran; ^bDepartment of Chemistry, University of Sistan and Baluchestan, Zahedan, Iran; ^cDepartment of Biology, University of Sistan and Baluchestan, Zahedan, Iran; ^dFaculty of Pharmacy, Zabol University of Medicinal Sciences, Zabol, Iran

Communicated by Ramaswamy H. Sarma

ABSTRACT

Better solubility and improved toxicity of palladium complexes compared with cisplatin were major reasons for synthesis of novel Pd(II) complex, [Pd(8Q)(bpy)]NO₃ (8Q=8-hydroxyquinolate, bpy=2,2'-bipyridine). Interaction between the [Pd(8Q)(bpy)]NO₃ complex and calf thymus DNA in aqueous solution has been investigated by circular dichroism (CD), UV-Visible absorption and fluorescence spectroscopic techniques. These experiments showed that prepared Pd(II) complex can effectively intercalate into CT-DNA and weakly bind to BSA in which the bovine serum albumin molecule was unfolded slightly. The cytotoxicity of the prepared complex has been evaluated on the MCF-7 and DU145 cell lines by MTT and TUNEL assay. The MTT results were showed that in DU145, the CC₅₀ values of [Pd(8Q)(bpy)]NO₃ and cisplatin are very close together (10.4 and 8.3 μM, respectively), unlike MCF-7. Accordingly, TUNEL assay was performed on DU145 and apoptosis was clearly obvious by 43% DNA fragmentation in the treated cell lines. So, we can suggest the [Pd(8Q)(bpy)]NO₃ as alternative drug for cisplatin in the future which has great potential in DNA denaturation and apoptosis specially on prostate cancer. PdO nanoparticles were successfully prepared without supported any surfactants via sonochemical approach. The synthesized PdONPs were characterized using UV-Vis and FTIR spectroscopy, X-ray diffraction (XRD), dynamic light scattering (DLS), energy-dispersive X-ray spectroscopy (EDX), scanning electron microscopy (SEM) and transmission electron microscopy (TEM).

Abbreviations: CT-DNA: Calf thymus deoxyribonucleic acid; BSA: Bovine Serum Albumin; CD: Circular Dichroism; K_{app}: Apparent binding constant; K_{sv}: Stern-Volmer constant; K_q: Quenching constant; EtBr: Ethidium Bromide; DLS: dynamic light scattering; SEM: Scanning Electron Microscopy; TEM: transmission electron microscopy; EDX: energy-dispersive X-ray spectroscopy; XRD: X-ray diffraction; MTT: 3-(4,5-Dimethylthiazol-2-Yl)-2,5-Diphenyltetrazolium Bromide

ARTICLE HISTORY

Received 17 July 2018
Accepted 23 October 2018

KEYWORDS

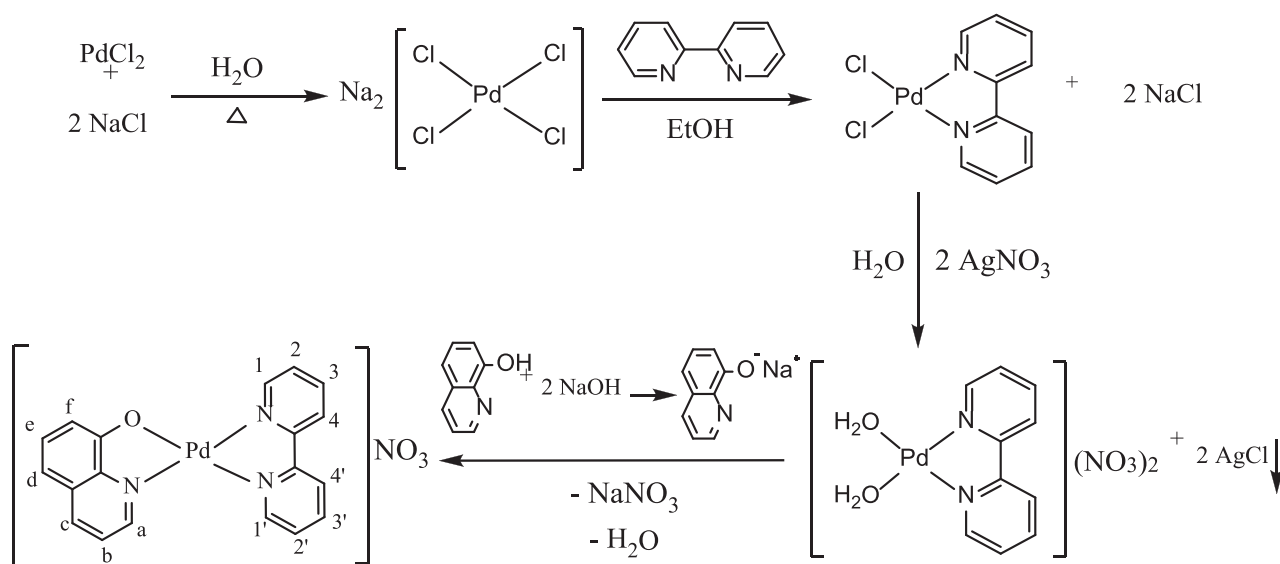
Pd(II) complex; cytotoxicity; DNA/BSA binding; 8-hydroxyquinoline; nanoparticle

1. Introduction

For several decades, identification of new cytotoxic compounds led to development of therapeutic agents for treatment of cancer. It is noticeable that less than 40 agents were routinely used in the clinical stage over 600,000 compounds in the testing phase, due to limitation of their application as antitumor drugs (Schwartzmann, Winograd, & Pinedo, 1988). In addition, application of some common anticancer drugs widely used in cancer therapy is limited because of their severe side effects. For example, cisplatin have several undesirable effects for patients including its toxicity to the brain, drug resistance, low stability and low solubility in physiological media. These limitations caused improvement in synthesis of new derivatives with anticancer activity

(Dahm, Bailly, Karmazin, & Bellemin-Lapponnaz, 2015; Liang et al., 2017).

Many palladium complexes were synthesized and characterized because of their structural similarity with platinum based drugs and anticancer properties, such as less kidney toxicity (Hadian Rasanani et al., 2018; Kelland, 2007; Mansouri-Torshizi, Moghaddam, Divsalar, & Saboury, 2009; Saeidifar et al., 2017; Ulukaya et al., 2011). Chelating ligands with N, O, S donor groups, such as phenanthroline derivatives, N-heterocyclic carbenes and Schiff bases enhanced the activity of Pd(II) complexes (Carvalho et al., 2015; Ray et al., 2007). This activity is also increased using lipophilic ligands which less by improved transferring through cell membranes (Hadjikakou & Hadjiliadis, 2009). 2,2'-bipyridine (bpy) as N,N-donor chelating ligand can form a planar complex with transition metal complexes and act



Scheme 1. Preparation route of $[\text{Pd}(8\text{Q})(\text{bpy})]\text{NO}_3$ complex with ^1H NMR numbering.

as DNA intercalator (Aminzadeh, Mansouri-Torshizi, & Modarresi-Alam, 2017; Guney, Yilmaz, & Kazak, 2010; Shahraki et al., 2014; Tomás-Mendivil, Díez, & Cadierno, 2013). Metal complexes bearing lipophilic ligands can bind to DNA which occurred by non-covalent interactions, such as both van der Waals and hydrophobic forces. During recent years, considerable attention has been directed toward 8-hydroxyquinoline (8Q) and derivatives because of diverse types of biological activities, such as antibacterial, antibiotic and antifungal efficiency (Mahamoud, Chevalier, Davin-Regli, Barbe, & Pages, 2006; Musiol et al., 2007; Palit et al., 2009). Recently, transition metal complexes containing 8Q derivatives have been reported and used with good anticancer activity (Mansouri-Torshizi, Rezaei, Kamranfar, & Majd, 2016; Mansouri-Torshizi, Saeidifar, Rezaei-Behbehani, Divsalar, & Saboury, 2010; Saeidifar et al., 2014; Sorinezami & Mansouri-Torshizi, 2016; Sorinezami, Mansouri-Torshizi, & Ghanbari, 2017).

Interaction studies of small molecules with DNA are important for further investigating of the structure and function of DNA and designing new drugs. Small molecules can bind to DNA by three kinds of non-covalent interactions, such as electrostatic binding, groove binding and intercalation binding modes (Chitrapriya, Jang, Kim, & Lee, 2011; Shi, Lou, Zhou, & Pan, 2018).

The drug-protein interaction in the blood stream, serum or plasma may cause to formation of a protein-drug complex that greatly influences on the distribution, metabolism and toxicity of drugs in the body. Albumin is one of the most numerous plasma protein in mammals with diverse functions in transportation of substances and in the metabolism and distribution of endogenous and exogenous molecules (Luo, Shi, Hu, Zhao, & Huang, 2012; Nicholson, Wolmarans, & Park, 2000; Shahraki, Shiri, Majd, & Razmara, 2017). Bovine serum albumin (BSA) is mainly selected as an adequate protein model for drug-protein interactions, due to its availability, relatively low cost, structural similarity with human serum albumin and high affinity binding sites to metal complexes (Eslami Moghadam et al., 2016; Milutinović et al., 2017; Shahraki, Shiri, & Saeidifar, 2018; Shiri, Shahraki, & Shahriari, 2018; Wang, Herting, Wallinder, & Blomberg, 2015).

During recent years, the interest for transition metal complexes bearing planar extended aromatic ligands has tremendously increased due to their application as probes capable to utilize the nucleic acid structures (Sun et al., 2016; Tarushi et al., 2017). This article reports the synthesis and characterization of a new water-soluble Pd (II) antitumor complex containing 2,2'-bipyridine (bpy) and 8Q as planar and aromatic chelating ligands. PdO nanoparticles were also prepared without using any surfactants via sonochemical approach which is an efficient method for production of desirable nano-materials with different morphologies and sufficient nanoparticles (Abbasian & Ghanbari, 2015; Ghanbari, Salavati-Niasari, & Ghasemi-Kooch, 2014). The synthesized PdONPs were characterized using UV-Vis spectroscopy, Fourier transform-infrared (FTIR) spectroscopy, X-ray diffraction (XRD), dynamic light scattering (DLS), energy-dispersive X-ray spectroscopy (EDX), scanning electron microscopy (SEM) and transmission electron microscopy (TEM).

Since design of new drugs that can intercalate in DNA is very important, we have designed a new Pd(II) complex which can intercalate from both sides (bpy or 8Q) between base pairs of DNA as both of the ligands are planar and aromatic, (Scheme 1). In addition, this complex is water soluble which is an important first step for possible applications in biological systems. In vitro cytotoxic activity of $[\text{Pd}(8\text{Q})(\text{bpy})]\text{NO}_3$ compared to cisplatin was investigated against both prostate cancer DU145 cells and breast cancer MCF-7 cells. The apoptotic effect of complex in DU145 cell lines was examined by TUNEL assay. Furthermore, the binding affinity toward the BSA as well as binding properties to CT-DNA have been evaluated by circular dichroism (CD), UV-Vis absorption spectroscopy and fluorescence quenching measurements.

2. Experimental

2.1. Materials

Palladium(II) chloride, sodium chloride, highly polymerized calf thymus DNA sodium salt (CT-DNA), 8Q, 2,2'-bipyridine, AgNO_3 , Tris-HCl buffer and (3-(4,5-dimethylthiazol-2-yl)-2, 5-

diphenyltetrazolium bromide (MTT) were purchased from Merck (Germany). Ethidium bromide (EtBr) and sephadex G-25 were obtained from Fluka (Switzerland). BSA was purchased from Aldrich Chemical Co (USA) and used as received. MCF-7 and DU145 cell lines were obtained from Pasteur Institute (Tehran, Iran). T-Octylphenoxypolyethoxyethanol (Triton X-100), Phosphate buffered saline powder, sodium citrate and paraformaldehyde were obtained from sigma (USA). TdT-mediated dUTP Nick-End Labeling (TUNEL) kit was bought from Roche Applied Science (Germany). All media and cell culture components were obtained from Life Technologies (USA). Solvents used were of reagent grade and purified before being used by the standard methods. The double-distilled water was used for preparation of all solutions.

2.2. Measurement instruments

Infrared spectrum of the metal complex was determined with KBr pellet on a JASCO-460 plus FT-IR spectrometer in the range of 4000–400 cm^{-1} . ^1H NMR spectrum of the complex was recorded with a Bruker AC-80 Avance spectrometer at 500 MHz in DMSO-d_6 using tetramethylsilane as internal reference. Electronic absorption spectra of $[\text{Pd}(8\text{Q})(\text{bpy})]\text{NO}_3$ complex were measured on a JASCO UV-Vis 7850 recording spectrophotometer and the fluorescence spectra were recorded on a Cary Eclipse spectrofluorimeter (Varian, USA). Circular dichroism (CD) spectra were measured on an Aviv Spectropolarimeter model 215 (USA) in a 1 mm path length cylindrical quartz cell. XRD analysis of the samples were carried out on a Bruker D8 ADVANCE X-ray diffractometer equipped with a Cu $\text{K}\alpha$ source ($\lambda = 0.154 \text{ nm}$) at 40 kV and 30 mA. Morphologies of samples were examined by HITACHI S-570 scanning electron microscopy (SEM). The elemental analysis of the prepared particles was also implemented by a SEM equipped with an energy-dispersive X-ray spectrum (EDX). The morphology of the prepared samples was characterized using Philips EM208 TEM with an accelerating voltage of 100 kV. The size distribution and zeta potential were carried out by DLS measurements using Zetasizer Nano S90 (Malvern Instruments Ltd., U.K.). Conductivity measurement of the Pd(II) complex was carried out on a Systronics conductivity bridge 305. Microchemical analysis of carbon, hydrogen and nitrogen for the complex was done using Heraeus CHNO-RAPID elemental analyzer. Treated cells were analyzed using Olympus IX81 compound fluorescence microscope equipped with XM10 monochrome camera (Olympus, Hamburg, Germany).

2.3 Synthesis of $[\text{Pd}(8\text{Q})(\text{bpy})]\text{NO}_3$

For the first step, 2,2'-bipyridinedichloropalladium(II), $[\text{Pd}(\text{bpy})\text{Cl}_2]$, was synthesized as described previously (Mansouri-Torshizi et al., 2016; Saaidifar, Mansouri-Torshizi, Divsalar, & Saboury, 2013). PdCl_2 (0.885 g, 5.0 mmol) and NaCl (2.922 g, 50 mmol) was dissolved in a 100 ml flask containing 100 ml distilled water and was stirred for 30 min at 60 °C. 2,2'-bipyridine (0.780 g, 5.0 mmol) was dissolved in

50 ml of water-ethanol mixture (1:1 v/v) and then added dropwise to the above solution while stirring vigorously. Stirring was continued for another 2 h at room temperature. The yellowish precipitate so obtained was filtered and washed several times with water, ethyl alcohol, and acetone and was dried at 40 °C. Yield was 1.53 g (92%). In the second step, for preparation of $[\text{Pd}(8\text{Q})(\text{bpy})]\text{NO}_3$ (Scheme 1), $[\text{Pd}(\text{bpy})\text{Cl}_2]$ (0.333 g, 1.0 mmol) was dispersed in 20 ml water, then NaHCO_3 (0.084 g, 1 mmol) and 8Q (0.145 g, 1.0 mmol), dissolved in 10 ml water, was added to this solution. The mixture was stirred at 45–50 °C for 2 h. Volume of the solution was increased to 60 ml with distilled water and then AgNO_3 (0.34 g, 2.0 mmol) was added and the solution was stirred at 55 °C in the dark for 7 h. Stirring was continued at room temperature in the dark for 10 h. The AgCl precipitate was filtered and the clear reddish filtrate was evaporated under vacuum to dryness at 35–40 °C. The orange powder so obtained was dissolved in 55 ml of acetonitrile-methanol (1:1 v/v) and then was filtered. The ether diffusion into the filtrate was resulted the dark orange microcrystals which formed after three days. The crystals were isolated by filtration, washed with 15 ml acetone, and dried at 40 °C (Yield: 0.31 g, 66.2%). All our attempts to grow single crystals were unsuccessful. Anal. Calcd. for $\text{C}_{18} \text{H}_{14} \text{N}_4 \text{O}_4 \text{Pd}$ (468 g/mol): C, 48.72; H, 2.99; N, 11.96%. Found: C, 48.70; H, 3.03; N, 12.01%. FT-IR spectrum of the Pd(II) complex shows five characteristic bands at 1108, 1319, 3059, 1608 and 1384 cm^{-1} assigned to $\nu(\text{C}=\text{O})$, $\nu(\text{C}=\text{N})$, $\nu(\text{C}-\text{H}$ aromatic), $\nu(\text{C}=\text{C}$ aromatic) and NO_3^- (uncoordinated counter ion) stretching modes, respectively (Nakamoto, 2008). ^1H NMR (500 MHz, DMSO-d_6 , ppm): Protons of quinoline moiety resonate at 6.42 (d, 1H, H-f), 6.86 (d, 1H, H-d), 7.13 (t, 1H, H-e), 7.55 (q, 1H, H-b), 8.15 (d, 1H, H-c), 8.24 (d, 1H, H-a) and the protons of 2,2'-bipyridine moiety resonate at 7.53 (t, 2H, H-2,2'), 8.12 (d, 2H, H-4,4'), 8.25 (t, 2H, H-3,3'), 8.31 (t, 2H, H-1,1'). ^1H NMR spectrum of the Pd(II) complex is shown in supplementary data, Figure 1s.

Electronic absorption spectrum of the Pd(II) complex shows four bands at 204 ($\log \epsilon = 3.60$) (I), 238 ($\log \epsilon = 3.25$) (II), 312 ($\log \epsilon = 2.74$) (III) and 396 nm ($\log \epsilon = 2.42$) (IV). Bands (I), (II) and (III) are assigned to the first and higher $\pi \rightarrow \pi^*$ transitions of 2,2'-bipyridine and 8-hydroxyquinoline ligands (Mansouri-Torshizi et al., 2010). However band (IV) show blue shift of 10 nm from less polar ethanol to more polar water. This band may be assigned to charge transfer from Pd(II) to 2,2'-bipyridine and 8-hydroxyquinoline ligands. The compound was decomposed at 256 °C. The preparation route is shown in Scheme (1).

2.4 Synthesis of PdONPs

The sonochemical synthesis of PdO nanoparticles were obtained by ultrasonic irradiation of $[\text{Pd}(8\text{Q})(\text{bpy})]\text{NO}_3$ compound. The complex was dissolved in 50 ml of water under ultrasonic waves (150 W, 30 min) followed by addition of sodium hydroxide as precipitating agent. The obtained product was characterized after calcination at 400 °C for 2 h.

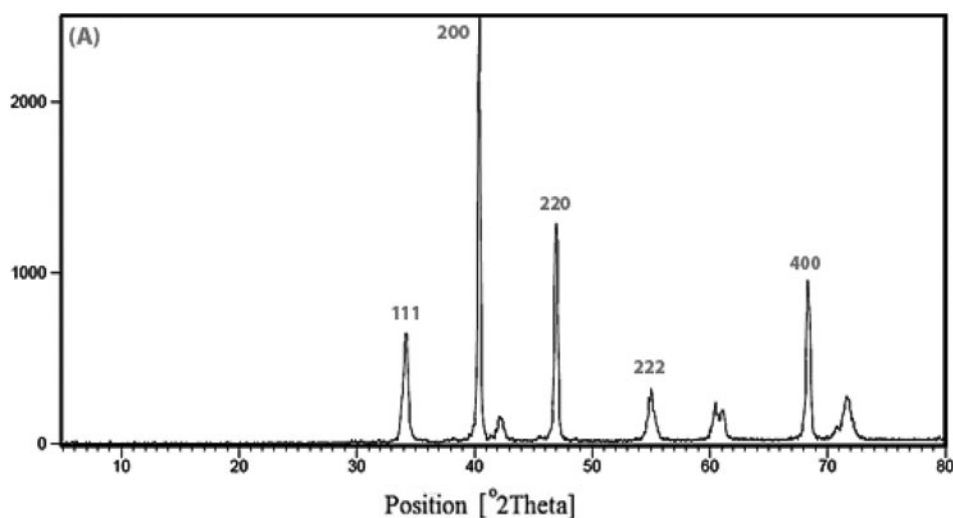


Figure 1. XRD patterns of PdO nanoparticles synthesized by sonochemical method.

2.5 Interaction with DNA and BSA

Earlier, we described the procedures of interaction studies between metal complexes with CT-DNA (Islami-Moghaddam, Mansouri-Torshizi, Divsalar, & Saboury, 2009). For interaction studies of our new complex, different UV absorption and fluorescence methods were used and stock solutions of Pd(II) complex (1.4 mM), CT-DNA (4 mg/mL) and BSA (10 μ M) were prepared in Tris-HCl buffer (20 mM, pH 7.0) containing 20 mM sodium chloride. The absorption titration measurements were studied at $\lambda_{\text{max}}=312$ (nm) and complex-DNA/BSA systems were incubated for 1 h both at 300 and 310 K, respectively, before spectral measurements. In the fluorescence measurements, the excitation wavelength were set at 471 and 295 nm and emission spectra were recorded in the range of 550–700 nm and 300–500 nm for CT-DNA and BSA systems, respectively. DNA concentrations were determined by UV spectrophotometry by absorption intensity at 260 nm using the molar absorption coefficient of DNA ($\epsilon_{260}=6600 \text{ M}^{-1} \text{ cm}^{-1}$) (Eslami Moghadam et al., 2016). CT-DNA solution gave a ratio of UV absorbance at 260 and 280 nm (A_{260}/A_{280}) of approximately 1.8–1.9 indicating that the DNA was sufficiently free of protein (Mansouri-Torshizi et al., 2010). The concentration of BSA solution was determined spectrophotometrically using $\epsilon_{280}=44,300 \text{ M}^{-1} \text{ cm}^{-1}$ (Alarcon et al., 2010). For CD measurements, each samples were scanned in the range of 200–350 nm in Tris-HCl buffer solution at ambient temperature. The spectral data were collected with [Complex]/[macro-molecule] ratio (1/R)=1, [DNA] = 50 μ M and [BSA] = 3 μ M.

2.6 Cell culture and in vitro cytotoxicity analysis: MTT assay

Prostate cancer DU145 cells and breast cancer MCF-7 cells were cultured at a seeding density of 4.0×10^4 cells/cm² into the T-50 flasks using RPMI 1640 media supplemented with 10% FBS, 100 units/mL penicillin G, and 100 mg/mL streptomycin (Heidari Majd, Akbarzadeh, & Sargazi, 2017; Sargazi, Kuhistani, Nosrat Nahoki, & Heidari Majd, 2015). The cultured cells were kept at 37 °C in a humidified CO₂ incubator during

cultivation and during experiments. Cytotoxicity assay was conducted in both DU145 and MCF-7 cells. Cells (1×10^4 cells/well) were cultivated onto 96-well plates. At 40–50% confluency (24 h post-seeding), the cultured cells were treated with different concentrations (i.e. ranging from 12.5 to 200 μ M) of Pd(II) complex and cisplatin as an anti-cancer drug. The treated cells were incubated for different time frames (i.e. 24, 48, and 72 h), and then subjected to 3-(4,5-dimethylthiazol-2-yl)-2,5-diphenyltetrazolium bromide (MTT). The media was removed and 150 μ L of fresh media plus 50 μ L MTT solutions (prepared as 2 mg/mL in FBS) were added to each well and incubated for 4 h at 37 °C in a CO₂ incubator. The media was removed and the cells were washed (3 \times), and then the formed formazan crystals were dissolved by adding DMSO (200 μ L) and Sorenson's buffer (25 μ L) to each well. The absorbance was read at 570 nm using a spectrophotometer (BioTek Instruments, Inc., Bad Friedrichshall, Germany).

2.7 Apoptotic study by TUNEL assay

DU145 cells were treated with 10.5 μ M of prepared palladium complex for 72 h. Cells were washed with phosphate buffered saline (PBS) and then control and treated cells were fixed in 4% paraformaldehyde in PBS for 1 h and rinsed (3 \times) with PBS. A solution containing 0.1 g Triton X-100 and 0.1 g sodium citrate in 100 mL of molecular grade H₂O was added for 15 min at RT to permeabilize the cells. After washing with PBS (3 \times), cells were incubated with TUNEL reaction mixture for 1 h at 37 °C in a humidified atmosphere in the dark. Cells were rinsed with PBS (3 \times) and the cells were photographed using fluorescent microscope. For quantification of apoptotic cells, a total of 200–400 cells were counted.

3. Results and discussion

3.1 Characterization of the complex

The new Pd(II) complex of formula [Pd(8Q)(bpy)]NO₃ (where bpy = 2,2'-bipyridine and 8Q = 8-hydroxyquinolate has

been synthesized by interaction of diaquo-2,2'-bipyridinepalladium(II) nitrate with sodium salt of 8Q. The molar conductance value of this complex in water is 108 ($\Omega^{-1} \text{ mol}^{-1} \text{ cm}^2$). This value is unchanged after 2 days and thus suggests that it is 1:1 electrolyte (Geary, 1971).

In spite of the presence of four aromatic rings in the structure of the complex, it is soluble enough in water being the first important step for possible applications in biological systems. This may be due to presence of a positive charge on complex ion being balanced by an ionizable NO_3^- acting as counter ion. Satisfactory results of spectral and elemental analysis revealed that the complex is of good purity. The analytical data of the complex are given in Section 2.3. Non-spectral (elemental analysis and conductivity measurement) and spectral (UV-Vis, FT-IR and ^1H NMR) characterization data, support the proposed structure of the metal complex shown in Scheme 1, where a bidentate coordination of both ligands are proposed. The crystalline phases and morphologies of the samples were characterized by XRD and scanning electron microscope (SEM). A detailed account of cytotoxic activity (CC_{50}), binding ($[\text{L}]_{1/2}$, m) and refolding/unfolding ability of the complex to CT-DNA and BSA are discussed in the following sections.

3.2 FT-IR spectra and XRD analysis

The FT-IR spectra of the prepared products without calcinations and after calcinations are shown in supplementary data, Figure 2s. FTIR spectrum of PdO nanoparticles exhibited peak at near 669 cm^{-1} , corresponding to the Metal–Oxygen stretching mode which is assigned to Pd–O bond in PdO (Kliche, 1985). The crystalline nature of the PdONPs was clarified with XRD analysis. The XRD pattern of PdO reveals the typical diffraction patterns of pure substance with characteristic reflection peaks, corresponding to the face-centered cubic structure of the crystalline Pd (JCPDS NO.: 046-121). Using Scherrer equation, $D_c = K\lambda/\beta \cos\theta$, where β is the width of the observed diffraction peak at its half maximum intensity, K is about 0.9, as the shape factor and λ is the X-ray wavelength (CuK α radiation, equals to 0.154 nm) was about 16.7 nm (Bayat, Ghanbari, & Salavati-Niasari, 2016). XRD pattern for sample including PdO nanoparticles are shown in Figure 1.

3.3 DLS measurements, SEM/TEM images and energy-dispersive X-ray spectrum (EDX)

The DLS measurement presented the size distribution of the PdO nanoparticles with an average size of about 126 nm. The zeta potential analysis showed that PdONPs had negative value (-64.4 mV) indicating that PdO nanoparticles possess negatively charged surface. The size obtained by the DLS is different because it gives the average size of the particles as well as non-homogeneous dispersion of the samples. SEM images of nanostructures synthesized by sonochemical approach are shown in Figure 2a, b, which implies nanostructures with average diameter of 56–119 nm were obtained. By applying ultrasonic waves at 180 W and 60 min, nano-products

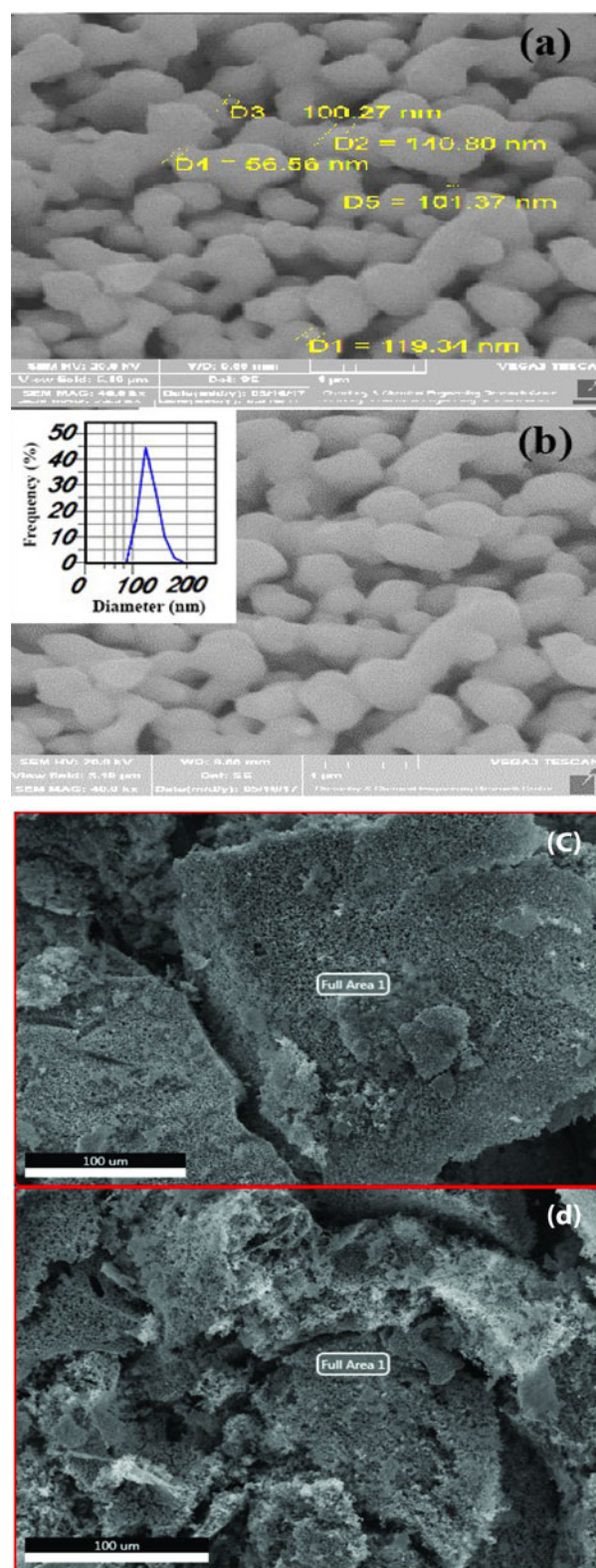


Figure 2. SEM images of PdO nanoparticles (a and b). TEM images of PdO nanoparticles (c and d). DLS diagram (b, inserted).

with lower particle size were synthesized. For better estimation of the particle size of nanoparticles, transmission electron microscopy (TEM) was used. TEM image of PdONPs is shown in Figure 2c, d that confirms synthesis of nanoparticles with average particle size of about 60 nm. The EDX analysis of nanoparticles prepared by ultrasonic-assisted process is also

appeared in the Figure 3. The EDX quantitative analysis confirms the nanostructure which consists of about 70.30 wt% Pd, 8.60 wt% sodium, and 21.00 wt% oxygen.

3.4 DNA refolding and BSA unfolding

The interaction of complexes with macromolecules (DNA or BSA) may cause electronic perturbations which can be observed through spectroscopic titrations (Arjmand & Aziz, 2009; Chaveerach, Meenongwa, Trongpanich, Soikum, & Chaveerach, 2010). For this experiment, the sample cell and the reference cell were filled with 1.8 ml of Tris-HCl buffer solution of CT-DNA (0.136 mM) and BSA (0.011 mM), respectively that the absorption of CT-DNA in this concentration was ~ 0.8 . Then, 25 μ l of [Pd(8Q)(bpy)]NO₃ (1.4 mM) was added to both sample and reference cuvette and after 3 min, the absorption spectra were recorded at 260 and 280 nm for CT-DNA and BSA, respectively. Addition of metal complex to

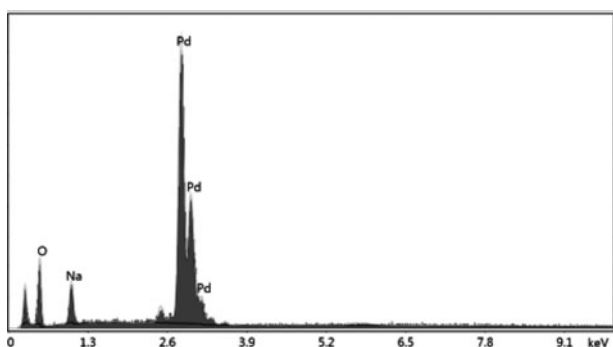


Figure 3. EDX of nanoparticles prepared by ultrasonic-assisted process.

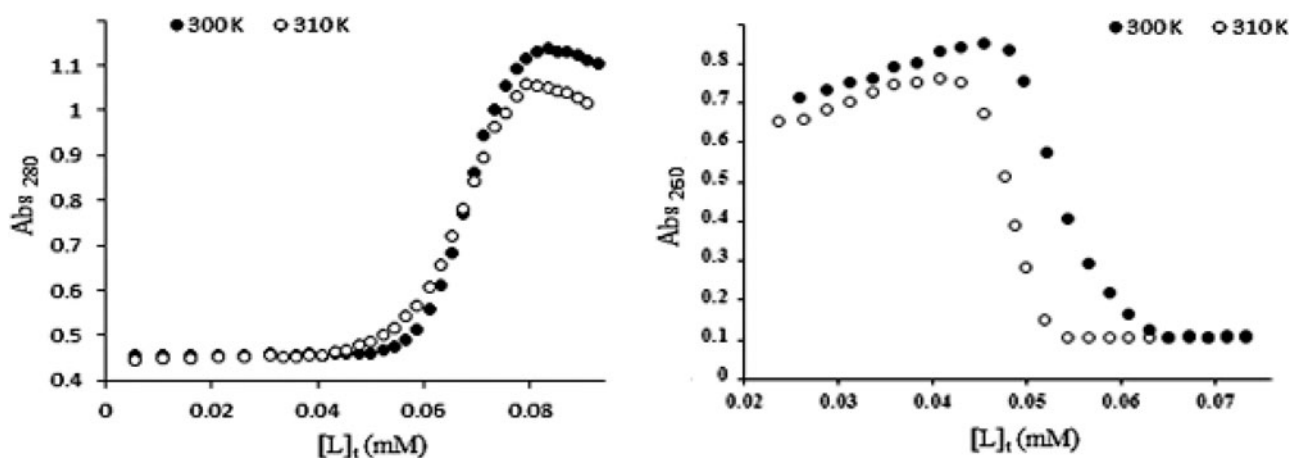


Figure 4. The changes in UV absorbance for CT-DNA (right) and BSA (left) due to increasing the total concentration of [Pd(8Q)(bpy)]NO₃, [L]_t at 300 and 310 K.

both cells was continued until no further changes were observed in the absorption readings. The experiment was examined at 300 and 310 K, separately. The conformational changes of native CT-DNA and BSA interaction by [Pd(8Q)(bpy)]NO₃ as a function of spectral changes at two temperatures (300 and 310 K) are illustrated in Figure 4, that shows an increase (left) and a decrease (right) in the absorption of fixed amount of CT-DNA and BSA respectively upon addition of increasing amount of [Pd(8Q)(bpy)]NO₃ complex. This behavior mirrored to refolding of CT-DNA and unfolding of BSA molecules. Refolding and unfolding causes hidden of purine and pyrimidine bases of CT-DNA and exposure of tryptophan residues of BSA to water molecules present in the medium leading to decrease in absorbance of CT-DNA and increase in absorbance of BSA.

The concentrations of Pd(II) complex in the midpoint of transition from native form to refolded (CT-DNA) or unfolded (BSA) by the Pd(II) complex, [L]_{1/2} value, are gathered in Table 1. The low values of [L]_{1/2} clearly confirmed the high ability of the [Pd(8Q)(bpy)]NO₃ complex, as a good anti-cancer drug, in modification of the native CT-DNA and BSA molecule.

3.5 Absorption titration measurements

This study provides a depth insight for interaction of physiological macromolecules with an antitumor metal complex. The calculated parameters may be useful for structural evaluation of the denatured macromolecules which are induced by the Pd(II) complex. In the first experiments a fixed amount of this complex (0.1 mM) was titrated with increasing

Table 1. Binding parameters for interaction between CT-DNA and BSA (data in bracket) with the [Pd(8Q)(bpy)]NO₃ complex in 20 mM Tris-HCl buffer and pH= 7.0.

Compound	Temp (K)	^a [L] _{1/2} (μM)	^b ΔA _{max}	^c g	^d K × 10 ⁴ (M) ⁻¹	^e n
[Pd(8Q)(bpy)]NO ₃	300 310	56 (66) 47 (60)	0.14 (0.48) 0.09 (0.37)	4 (4) 4 (4)	6.02 (4.56) 7.12 (7.93)	5.27 (5.25) 5.41 (4.36)

^aThe concentrations of the complex in the midpoint of transition.

^bChange in the absorbance when all the binding sites on DNA were occupied by metal complex.

^cThe number of binding sites per 1000 nucleotides.

^dThe apparent binding constant.

^eThe Hill coefficient (as a criterion of cooperativity).

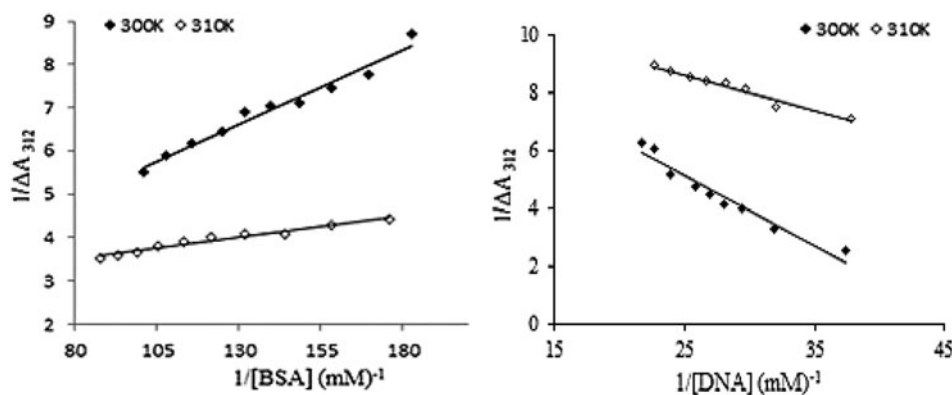


Figure 5. The changes in the absorbance of fixed amount of metal complex in the interaction with varying amount of macromolecules at 300 K and 310 K. The linear plot of the reciprocal of ΔA vs the reciprocal of [DNA] (right) and [BSA] (left) for the complex $[\text{Pd}(8\text{Q})(\text{bpy})]\text{NO}_3$.

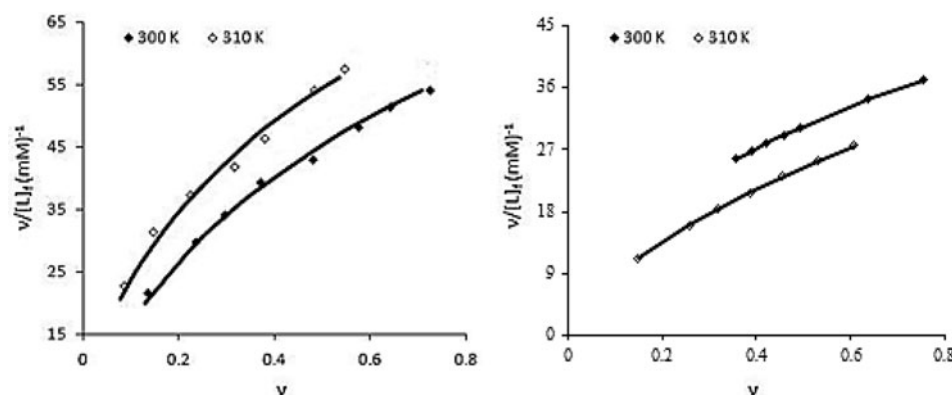


Figure 6. Scatchard plots for binding of the complex $[\text{Pd}(8\text{Q})(\text{bpy})]\text{NO}_3$ to CT-DNA (right) and BSA (left) at constant temperatures of 300 K and 310 K.

concentration of DNA or BSA at two temperatures, 300 and 310 K, and spectral changes are monitored based on UV-Vis technique. The values of ΔA_{max} in which all binding sites on DNA and or BSA are bound by the complex, are determined which are shown in Figure 5 and Table 1.

In the next experiments a fixed amount of each macromolecule was titrated with varying amounts of the Pd(II) complex at 300 and 310 K, separately. As shown in Figure 6, the Scatchard plots for the interaction of the Pd(II) complex with DNA or BSA are given using the values of $v/[L]_f$ versus v , where $[L]_f$ is the concentration of free metal complex, and v is the ratio of the concentration of bound metal complex to total DNA or BSA concentration (Scatchard, 1949). At both temperatures, the positive slope is observed in the plots, suggesting cooperative binding properties during interaction (Saeidifar et al., 2013).

To obtain the binding parameters, the above experimental data (v and $[L]_f$) were substitute in the following equation (Hill equation; Hill, 1910).

$$v = g(K[L]_f)^n / (1 + K[L]_f)^n \quad (1-3)$$

Using Eureka software to resolve the above equation, the theoretical values of unknown parameters (g , n , K) can be extracted, as shown in Table 1.

The values of n were calculated as 5.27 and 5.41 at 300 and 310 K, respectively indicating cooperative DNA binding with identical binding site (Shahraki, Shiri, Majd, & Razmara, 2017; Shiri, Shahraki, Baneshi, Nejati-Yazdinejad, & Majd,

2016; Shiri, Shahraki, Shahriyar, & Majd, 2017). The calculated apparent binding constant are comparable with those of 2,2'-bipyridine-palladium complexes reported earlier, acting as DNA intercalators (Aminzadeh et al., 2017; Saeidifar et al., 2014).

3.6 Fluorescence spectroscopic studies

Fluorescence spectroscopy is the most important technique to study the interaction of probes with macromolecules because of high sensitivity. The DNA binding of the $[\text{Pd}(8\text{Q})(\text{bpy})]\text{NO}_3$ complex was explored using competitive ethidium bromide (EtBr) binding experiments in Tris-HCl buffer solution at pH = 7.0. It is well known that upon binding to DNA, the fluorescence intensity of EtBr is significantly increased due to its strong intercalation between the DNA base pairs (Kumar & Arunachalam, 2007; Olmsted III & Kearns, 1977). Addition of Pd(II) complex to the EtBr-DNA system, resulted in gradually decrease in fluorescence intensity due to replacement of the EtBr molecule by the complex (Liu, Yuan, Zhang, Yan, & Yang, 2008). The emission spectra of EtBr bound to CT-DNA in the absence and the presence of the compound are given in Figure 7. In this figure, a weak intensity spectrum due to free EtBr near the base line is present. This implies that, in the competition between the two probes, the EtBr and Pd(II) complex, intercalation affinity of the Pd(II) complex is more than that of EtBr which cause releasing of EtBr molecules from CT-DNA.

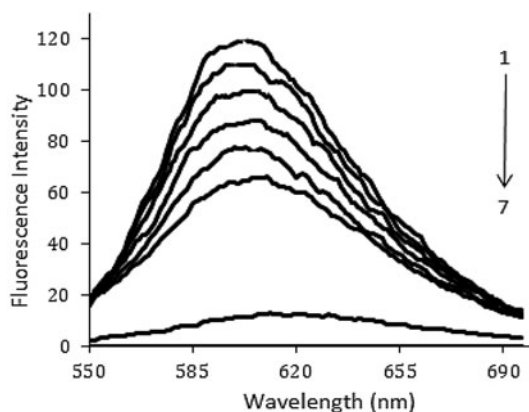


Figure 7. Fluorescence emission spectra of interacted EtBr-DNA in the absence (1) and presence of different concentration of the palladium(II) complex: 5 μM (2), 10 μM (3), 15 μM (4), 20 μM (5), 25 μM (6), EtBr alone (7).

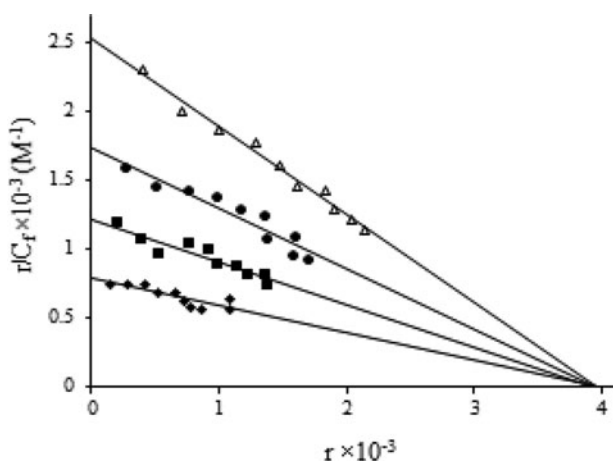


Figure 8. Competition between the complex $[\text{Pd}(8\text{Q})(\text{bpy})]\text{NO}_3$ with EtBr for the binding sites of DNA (Scatchard plot). In curve no. 1 (Δ), Scatchard's plot was obtained with calf thymus alone, $[\text{DNA}] = 60 \mu\text{M}$. In curves nos. 2 (\bullet), 3 (\blacksquare) and 4 (\blacklozenge) respectively, 30, 80 and 120 μM of $[\text{Pd}(8\text{Q})(\text{bpy})]\text{NO}_3$, were added, corresponding to molar ratio $[\text{complex}]/[\text{DNA}]$ of 0.017, 0.034 and 0.05. Solution were made in 20 mM NaCl, 20 mM Tris-HCl (pH = 7.0).

In addition, to characterize the mode of binding of $[\text{Pd}(8\text{Q})(\text{bpy})]\text{NO}_3$ to DNA, Scatchard analysis were carried out in which the number of EtBr molecules intercalated to DNA in the presence of different concentrations of the Pd(II) complex was calculated (Scatchard, 1949). For this purpose, appropriate amount of Pd(II) complex was added to the solution of CT-DNA pretreated with EtBr. The samples were incubated for 2 h and finally processed for fluorescence spectral measurements. The fluorescence scatchard plots were constructed for EtBr-DNA solution at different r_f values (as defined $[\text{Pd(II) complex}]/[\text{DNA}]$) as shown in Figure 8 and the results are summarized in Table 2. These values are comparable with those observed for the analogous complexes (Mansouri-Torshizi et al., 2010).

Figure 8 shows increasing the concentration of Pd(II) complex, decreases the value of K_{app} (i.e. apparent association constant) while the number of binding sites, n , is remain constant. This mode of DNA binding (type-A behavior) implies that the complex inhibits the EtBr binding to CT-DNA, competitively (Howe-Grant, Wu, Bauer, & Lippard, 1976).

Table 2. Binding parameters for the palladium(II) complex on the fluorescence of EtBr in the presence of CT-DNA.

Compound	$^a r_f$	$^b K \times 10^{-5} (\text{M})^{-1}$	$^c n$
$[\text{Pd}(8\text{Q})(\text{bpy})]\text{NO}_3$	0.000	0.574	0.004
	0.017	0.351	
	0.034	0.264	
	0.050	0.206	

^aFormal ratio of metal complex to nucleotide concentration.

^bAssociation constant.

^cNumber of binding sites per nucleotide.

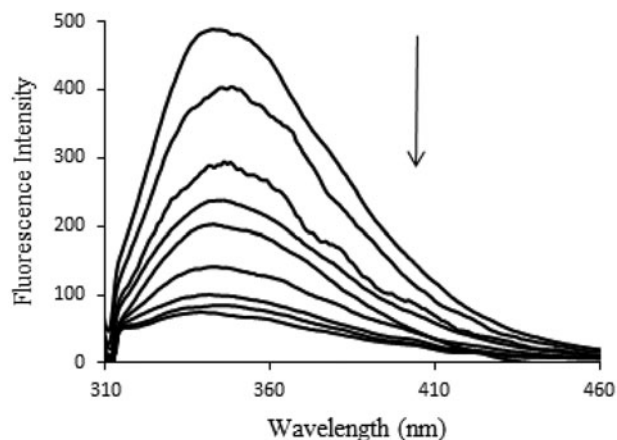


Figure 9. Fluorescence emission spectra of BSA (8 μM) in the absence and presence of different concentrations of the $[\text{Pd}(8\text{Q})(\text{bpy})]\text{NO}_3$ complex in a Tris-HCl buffer ($\lambda_{\text{max}} = 295 \text{ nm}$). The arrow shows the changes in emission intensity upon increasing the concentrations of the Pd(II) complex.

The characteristic fluorescence emission behavior of BSA is originated from Trp-134 and Trp-212 residues that provide the study of protein-small molecules interaction with fluorescence spectroscopic method (Messori, Orioli, Vullo, Alessio, & Iengo, 2000; Wang et al., 2011). Figure 9 shows the emission spectra of the BSA in the absence and presence of the $[\text{Pd}(8\text{Q})(\text{bpy})]\text{NO}_3$ complex at ambient temperature. A fixed concentration of BSA (8 μM), was titrated by various amounts of the Pd(II) complex (0.0–3.2 μM). Upon BSA binding of the Pd(II) complex, the emission intensity maximum at 345 nm is remarkably decreased without any significant change in the position of the maximum emission wavelength. The binding of the complex to BSA also quenches the intrinsic fluorescence attributed to the tryptophan residues in BSA (Hu, Liu, Pi, & Qu, 2005). The linear Stern-Volmer quenching constant for serum albumins has been measured from the following equation:

$$\frac{F_0}{F} = 1 + k_q \tau_0 [Q] = 1 + K_{\text{sv}} [Q] \quad (2-3)$$

where F_0 and F are the fluorescence intensities in the absence and presence of quencher respectively, K_{sv} is the Stern-Volmer quenching constant and $[Q]$ is concentration of quencher, k_q is the bimolecular quenching rate constant and equal to $k_q = K_{\text{sv}}/\tau_0$, and τ_0 is the average lifetime of the BSA in the absence of quencher. The value of τ_0 is equal to 10^{-8} s for tryptophan fluorescence in proteins (Zhang, Ma, Wang, Zhang, & Zhou, 2012). The plot of F_0/F versus $[Q]$ should gave a straight line with a slope equal to Stern-Volmer quenching constant. The value of K_{sv} was obtained $6.29 \times 10^5 \text{ M}^{-1}$ for Pd(II) complex (Figure 10).

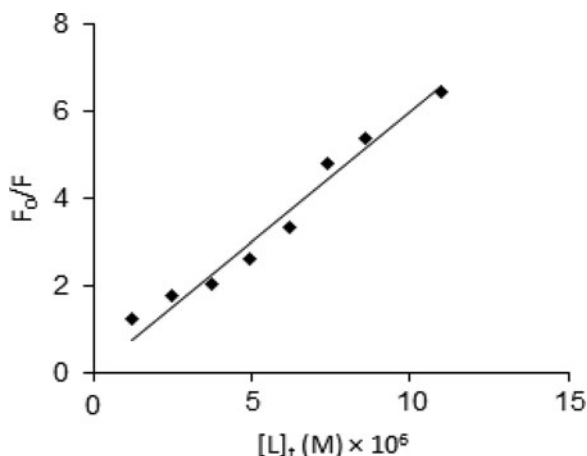


Figure 10. The Stern–Volmer curve of the fluorescence quenching of BSA by [Pd(8Q)(bpy)]NO₃ complex in Tris-HCl buffer at 300 K.

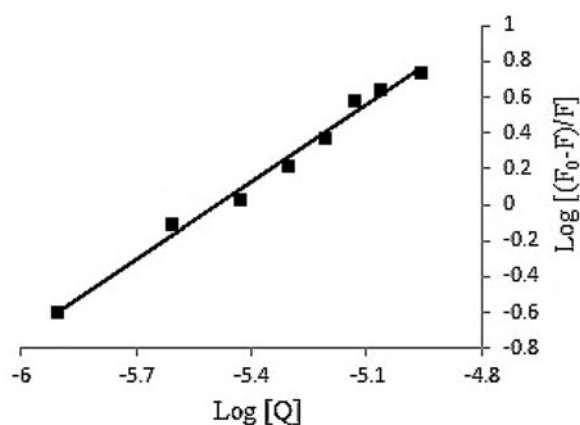


Figure 11. Plot of $\log[(F_0-F)/F]$ vs. $\log[Q]$ for determination of the Pd(II) complex-BSA binding constant and the number of binding sites on BSA.

Moreover, fluorescence quenching phenomena is classified into two important quenching mechanisms, the dynamic and static quenching. The value of k_q was calculated as $6.29 \times 10^{13} \text{ M}^{-1} \text{ s}^{-1}$, which is greater than the maximum diffusion collision rate constant ($2.0 \times 10^{10} \text{ M}^{-1} \text{ s}^{-1}$) for a biomolecules, suggesting the existence of static quenching process during BSA binding of the Pd(II) complex (Ramachandran, Raja, Bhuvanesh, & Natarajan, 2013). To evaluate the binding constant (K_A) and the number of the Pd(II) complex bound per protein (n), the following equation was used for static quenching mechanism (Cui et al., 2003):

$$\text{Log} \frac{(F_0-F)}{F} = \text{Log} K_{\text{bin}} + n \text{Log} [Q] \quad (3-3)$$

where K_{bin} is the apparent binding constant for the formation of BSA–drug complex, n is the number of the binding sites on the BSA molecule and $[Q]$ and $[P]_t$ are total concentration of quencher and protein, respectively. By plotting of $\text{Log} \frac{(F_0-F)}{F}$ versus $\text{Log} [Q]$ the values of K_{bin} and n are obtained from the intercept and slope, respectively (Figure 11). The calculated K_{bin} and n values for the BSA–complex system are presented in Table 3.

The results indicate that the value of apparent association constant for Pd(II) complex is higher than that of the Stern-Volmer quenching constant. This implies that static

Table 3. Quenching constant (K_{sv}), binding constant (K_{bin}) and number of binding sites (n) for BSA interaction of the [Pd(8Q)(bpy)]NO₃ complex.

Complex	$K_{\text{sv}} (\text{M}^{-1})$	$K_q (\text{M}^{-1} \text{s}^{-1})$	$K_{\text{bin}} (\text{M}^{-1})$	n
[Pd(8Q)(bpy)]NO ₃	6.29×10^5	6.29×10^{13}	6.87×10^5	1.23

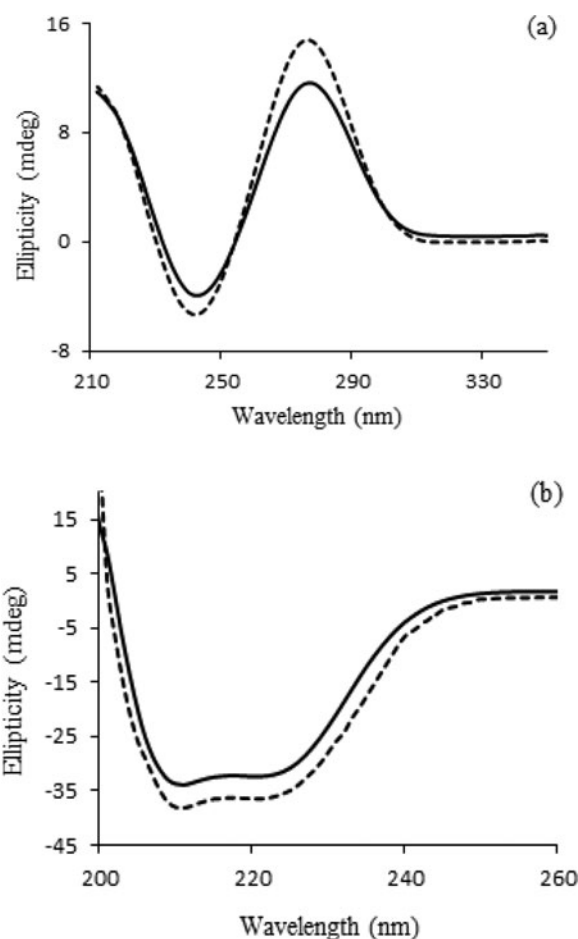


Figure 12. (a) CD spectra of CT-DNA (50 μM) in the absence (dashed line) and presence (solid line) of the Pd(II) complex. (b) CD spectra of free BSA (dashed line) and Pd-BSA system (solid line); [BSA] = 3 μM .

quenching is the possible mechanism in the binding process between BSA and complex.

3.7 CD spectral studies

CD spectroscopy is a quite sensitive technique in biological chemistry and structural biology to investigate the changes in macromolecule morphology during interaction with small molecules. The CT-DNA in right-handed B form is characterized in CD spectrum by a positive band at 275 nm due to base stacking and also a negative band at around 247 nm correlated to helicity (Loganathan et al., 2012). By addition of the Pd(II) complex to the DNA solution the intensities of both positive and negative CD bands are clearly decreased, which supporting the intercalation mode of interaction between the complex and DNA (Behnamfar et al., 2015). The CD spectra of CT-DNA in the absence and presence of Pd(II) complex are displayed in Figure 12a.

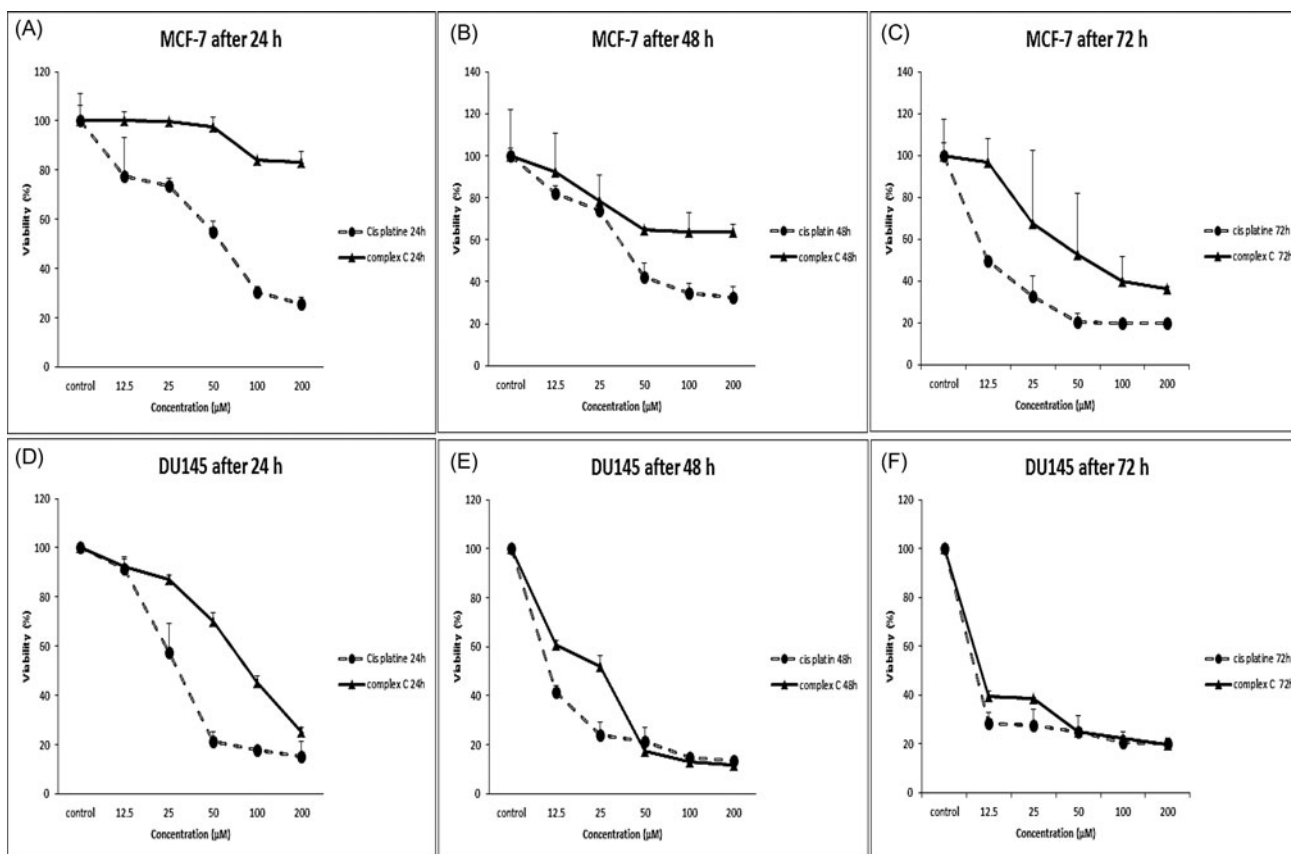


Figure 13. The impact of $[\text{Pd}(8\text{Q})(\text{bpy})]\text{NO}_3$ in the breast cancer MCF-7 cells (panel A–C) and prostate cancer DU145 cells (panel D–F).

In order to obtain an insight into the structure of the BSA, CD spectra are also monitored to examine the conformational aspects in BSA molecule upon environmental perturbations due to the interaction with Pd(II) complex. The CD spectrum of BSA exhibited two negative peaks at 208 and 222 nm, which is characteristic of the α -helix structure of the protein. Upon BSA interaction of the complex, the intensity of both negative peaks is decreased without any obvious shift of the bands indicating the unfolding of the peptide strand in protein secondary structure. The CD spectra were recorded in the absence and presence of the Pd(II) complex that are shown in Figure 12b which clearly showed that the α -helical content in the BSA protein is decreased upon interaction with metallodrug. The α -helix content of BSA before and after the addition of the Pd(II) complex is evaluated from MRE value at 208 nm according to the following equation (Chen, Yang, & Martinez, 1972):

$$\alpha - \text{helix}(\%) = \frac{-\text{MRE}_{208} - 4000}{33000 - 4000} \times 100 \quad (4-3)$$

where MRE_{208} is the experimental MRE values at 208 nm. The MRE value for pure is 33,000 and its value for β -form and random coil conformation is 4000 at 208 nm. The MRE_{208} , used to express variations in the secondary structure of BSA molecule are calculated by the following equation:

$$\text{MRE}_{208} = \frac{\text{observedCD}(m\text{deg})_{208}}{C_p \times n \times l \times 10} \quad (5-3)$$

where n is the number of amino acid residues (for BSA molecule is equal to 583), C_p is the molar concentration of BSA, l

is the cell path length (1 mm). The results showed that with addition of the Pd(II) complex decreasing tendency of the α -helix content from 55.21 to 48.82% is observed.

3.8 In vitro effects of Pd(II) complex and cisplatin on MCF-7 and DU145 cell lines

Forasmuch as the cytotoxicity of palladium complexes against human breast cancer cell lines and prostate cancer cell lines has been confirmed (Khan et al., 2011; Ulukaya et al., 2011), the MCF-7 and DU145 cell lines were selected for cytotoxicity evaluation of $[\text{Pd}(8\text{Q})(\text{bpy})]\text{NO}_3$ in comparison to cisplatin. Figure 13 represents the impact of $[\text{Pd}(8\text{Q})(\text{bpy})]\text{NO}_3$ in the breast cancer MCF-7 cells (panel A–C) and prostate cancer DU145 cells (panel D–F). In DU145 cells, Pd(II) complex resulted in prolonged inhibitory up to 72 h in sustained manner compared to cisplatin (about 80% toxicity for Pd(II) complex). In MCF-7 cells, the cytotoxic effects of $[\text{Pd}(8\text{Q})(\text{bpy})]\text{NO}_3$ were partly low after 72 h in compared to DU145 (i.e. ~60–65% toxicity). In DU145 cells, the CC_{50} values of $[\text{Pd}(8\text{Q})(\text{bpy})]\text{NO}_3$ and cisplatin were evaluated 10.4 and 8.3 μM , respectively. But In MCF-7 cells, the CC_{50} value of the Pd(II) complex was very different with the cisplatin: 70 and 12.5 μM , respectively. The cytotoxic effect of $[\text{Pd}(8\text{Q})(\text{bpy})]\text{NO}_3$ on breast cancer cells seems to be time dependent, while it display a trend of time and concentration dependent inhibitory effects on prostate cancer cells. Similar to our results, Khan et al. (2011) have reported that

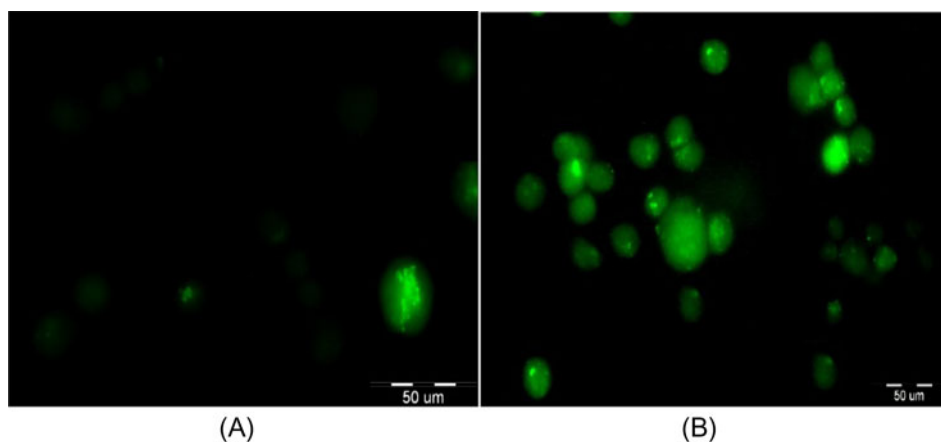


Figure 14. Assessment of apoptosis by TUNEL assay in DU145 cells. (a) Untreated cells. (b) The cells were exposed to 10.5 μM of $[\text{Pd}(8\text{Q})(\text{bpy})]\text{NO}_3$ for 72 h.

their new synthesized Pd(II) complexes are highly effective against DU145 cells.

3.9 Apoptosis assay

According to previous evidence, $[\text{Pd}(8\text{Q})(\text{bpy})]\text{NO}_3$ showed good cytotoxic effects on DU145 prostate cancer cells. To determine whether the cell death was attributable to $[\text{Pd}(8\text{Q})(\text{bpy})]\text{NO}_3$ -induced apoptosis, TUNEL assays were performed (Yang et al., 2015) for the course of 72 h treatment with 10.5 μM $[\text{Pd}(8\text{Q})(\text{bpy})]\text{NO}_3$ (CC_{50} value of Pd(II) complex). As shown in Figure 14, a detectable level of apoptosis was evident in DU145 cells after treatment with prepared Pd(II) complex in compared to untreated cells. After counting the apoptotic cells, nearly 43% of cells were dead after treatment with 10.5 μM of prepared palladium complex for 72 h. Based on similar work done by Ulukaya et al. palladium complex has showed extensive growth-inhibitory effect against prostate cancer cells (Ulukaya et al., 2013). They claimed that the palladium complex induced DNA damage and also cell death in prostate cancer cells. As well, induction of apoptosis was observed in prostate cancer DU145 cells after the treatment with $[\text{Pd}(8\text{Q})(\text{bpy})]\text{NO}_3$ on the basis of the TUNEL method.

4. Conclusions

In this article, a novel complex of Pd(II) was synthesized, characterized by elemental analysis, conductance and various spectral techniques. PdO nanoparticles were also prepared using this complex as a new precursor without using any surfactants, ligands as a capping agent lead to formation of nanoparticles. SEM/TEM images confirmed that nanostructures were obtained by sonochemical-assisted reactions. The DNA/BSA binding studies was investigated by CD measurements, UV-Vis and fluorescence methods. These studies confirm that the Pd(II) complex binds to double strand CT-DNA by the intercalation mode. This complex unexpectedly refolded CT-DNA at very low concentration. In addition, the in vitro interaction of Pd(II) complex with BSA has been investigated under simulated physiological conditions (pH 7.0) using spectroscopic methods. The results showed that the prepared Pd(II) complex weakly unfolded the peptide

strands of the BSA. On the other hand, according to cytotoxicity studies, the apoptosis ability of the $[\text{Pd}(8\text{Q})(\text{bpy})]\text{NO}_3$ on prostate cancer cells was confirmed. All these studies prompted us to propose this novel palladium complex as a potential therapeutic compound for the treatment of the cancer cells.

Acknowledgments

The authors are grateful for all support provided by University of Sistan and Baluchestan, University of Zabol and Zabol University of Medical science.

References

- Abbasian, H., & Ghanbari, D. (2015). Humidity sensing properties of $\text{Ni}(\text{OH})_2$ nanoparticles synthesized via sonochemical method. *Physica E: Low-Dimensional Systems and Nanostructures*, 65, 106–109. doi: 10.1016/j.physe.2014.09.001
- Alarcon, E., Aspée, A., Gonzalez-Bejar, M., Edwards, A., Lissi, E., & Scaiano, J. (2010). Photobehavior of merocyanine 540 bound to human serum albumin. *Photochemical and Photobiological Sciences*, 9(6), 861–869.
- Aminzadeh, M., Mansouri-Torshizi, H., & Modarresi-Alam, A. R. (2017). 2,2'-bipyridine coplanar with coordination square of Pd(II) nonylthiocarbamate antitumor complex interacting with DNA in two distinct steps. *Journal of Biomolecular Structure and Dynamics*, 35(11), 2301–2313. doi:10.1080/07391102.2016.1220328
- Arjmand, F., & Aziz, M. (2009). Synthesis and characterization of dinuclear macrocyclic cobalt(II), copper(II) and zinc(II) complexes derived from 2,2,2',2'-S,S[bis(bis-N,N-2-thiobenzimidazoloxalato-1,2-ethane)]: DNA binding and cleavage studies. *European Journal of Medicinal Chemistry*, 44(2), 834–844. doi:10.1016/j.ejmech.2008.05.006
- Bayat, S., Ghanbari, D., & Salavati-Niasari, M. (2016). Pechini synthesis of Co_2SiO_4 magnetic nanoparticles and its application in photo-degradation of azo dyes. *Journal of Molecular Liquids*, 220, 223–231. doi: 10.1016/j.molliq.2016.04.066
- Behnamfar, M. T., Hadadzadeh, H., Simpson, J., Darabi, F., Shahpiri, A., Khayamian, T., ... Salimi, M. (2015). Experimental and molecular modeling studies of the interaction of the polypyridyl Fe(II) and Fe(III) complexes with DNA and BSA. *Spectrochimica Acta Part A: Molecular and Biomolecular Spectroscopy*, 134, 502–516. doi:10.1016/j.saa.2014.06.105
- Carvalho, M. A., Arruda, E. G., Profirio, D. M., Gomes, A. F., Gozzo, F. C., Formiga, A. L., & Corbi, P. P. (2015). Chemical and spectroscopic characterizations, ESI-QTOF mass spectrometric measurements and DFT studies of new complexes of palladium(II) with tryptamine and mefenamic acid. *Journal of Molecular Structure*, 1100, 6–13. doi:10.1016/j.molstruc.2015.07.020

- Chaveerach, U., Meenongwa, A., Trongpanich, Y., Soikum, C., & Chaveerach, P. (2010). DNA binding and cleavage behaviors of copper(II) complexes with amidino-O-methylurea and N-methylphenyl-amidino-O-methylurea, and their antibacterial activities. *Polyhedron*, 29(2), 731–738. doi:10.1016/j.poly.2009.10.031
- Chen, Y.-H., Yang, J. T., & Martinez, H. M. (1972). Determination of the secondary structures of proteins by circular dichroism and optical rotatory dispersion. *Biochemistry*, 11(22), 4120–4131. doi:10.1021/bi00772a015
- Chitrapriya, N., Jang, Y. J., Kim, S. K., & Lee, H. (2011). Non-intercalative binding mode of bridged binuclear chiral Ru(II) complexes to native duplex DNA. *Journal of Inorganic Biochemistry*, 105(12), 1569–1575. doi:10.1016/j.jinorgbio.2011.08.016
- Cui, F.-L., Fan, J., Ma, D.-L., Liu, M.-C., Chen, X.-G., & Hu, Z.-D. (2003). A study of the interaction between a new reagent and serum albumin by fluorescence spectroscopy. *Analytical Letters*, 36(10), 2151–2166. doi:10.1081/AL-120023708
- Dahm, G., Bailly, C., Karmazin, L., & Bellemin-Lapponnaz, S. (2015). Synthesis, structural characterization and in vitro anti-cancer activity of functionalized N-heterocyclic carbene platinum and palladium complexes. *Journal of Organometallic Chemistry*, 794, 115–124. doi:10.1016/j.jorganchem.2015.07.003
- Eslami Moghadam, M., Saidifar, M., Divsalar, A., Mansouri-Torshizi, H., Saboury, A. A., Farhangian, H., & Ghadamgahi, M. (2016). Rich spectroscopic and molecular dynamic studies on the interaction of cytotoxic Pt(II) and Pd(II) complexes of glycine derivatives with calf thymus DNA. *Journal of Biomolecular Structure and Dynamics*, 34(1), 206–222. doi:10.1080/07391102.2015.1015056
- Geary, W. J. (1971). The use of conductivity measurements in organic solvents for the characterisation of coordination compounds. *Coordination Chemistry Reviews*, 7(1), 81–122. doi:10.1016/S0010-8545(00)80009-0
- Ghanbari, D., Salavati-Niasari, M., & Ghasemi-Kooch, M. (2014). A sonochemical method for synthesis of Fe₃O₄ nanoparticles and thermal stable PVA-based magnetic nanocomposite. *Journal of Industrial and Engineering Chemistry*, 20(6), 3970–3974. doi:10.1016/j.jiec.2013.12.098
- Guney, E., Yilmaz, V. T., & Kazak, C. (2010). Bis(saccharinato) palladium(II) and platinum(II) complexes with 2,2'-bipyridine: Syntheses, structures, spectroscopic, fluorescent and thermal properties. *Polyhedron*, 29(4), 1285–1290. doi:10.1016/j.poly.2010.01.006
- Hadian Rasanani, S., Eslami Moghadam, M., Soleimani, E., Divsalar, A., Ajloo, D., Tarlani, A., & Amiri, M. (2018). Anticancer activity of new imidazole derivative of 1R,2R-diaminocyclohexane palladium and platinum complexes as DNA fluorescent probes. *Journal of Biomolecular Structure and Dynamics*, 36(12), 3058–3076. doi:10.1080/07391102.2017.1385538
- Hadjivakou, S. K., & Hadjiliadis, N. (2009). Antiproliferative and anti-tumor activity of organotin compounds. *Coordination Chemistry Reviews*, 253(1-2), 235–249. doi:10.1016/j.ccr.2007.12.026
- Heidari Majd, M., Akbarzadeh, A., & Sargazi, A. (2017). Evaluation of host-guest system to enhance the tamoxifen efficiency. *Artificial Cells, Nanomedicine and Biotechnology*, 45(3), 441–447. doi:10.3109/21691401.2016.1160916
- Hill, A. V. (1910). The possible effects of the aggregation of the molecules of haemoglobin on its dissociation curves. *Journal of Physiology (London)*, 40, 4–7
- Howe-Grant, M., Wu, K. C., Bauer, W. R., & Lippard, S. J. (1976). Binding of platinum and palladium metallointercalation reagents and antitumor drugs to closed and open DNAs. *Biochemistry*, 15(19), 4339–4346. doi:10.1021/bi00664a031
- Hu, Y.-J., Liu, Y., Pi, Z.-B., & Qu, S.-S. (2005). Interaction of cromolyn sodium with human serum albumin: A fluorescence quenching study. *Bioorganic and Medicinal Chemistry*, 13(24), 6609–6614. doi:10.1016/j.bmc.2005.07.039
- Islami-Moghaddam, M., Mansouri-Torshizi, H., Divsalar, A., & Saboury, A. (2009). Synthesis, characterization, cytotoxic and DNA binding studies of diimine platinum(II) and palladium(II) complexes of short hydrocarbon chain ethyldithiocarbamate ligand. *Journal of the Iranian Chemical Society*, 6(3), 552–569. doi:10.1007/BF03246535
- Kelland, L. (2007). The resurgence of platinum-based cancer chemotherapy. *Nature Reviews Cancer*, 7(8), 573–584. doi:10.1038/nrc2167
- Khan, H., Badshah, A., Murtaz, G., Said, M., Rehman, Z.-U., Neuhausen, C., ... Butler, I. S. (2011). Synthesis, characterization and anticancer studies of mixed ligand dithiocarbamate palladium(II) complexes. *European Journal of Medicinal Chemistry*, 46(9), 4071–4077. doi:10.1016/j.ejmech.2011.06.007
- Kliche, G. (1985). Far-infrared reflection spectra of PdO, PdS, PdSe and PtS. *Infrared Physics*, 25(1-2), 381–383. doi:10.1016/0020-0891(85)90111-3
- Kumar, R. S., & Arunachalam, S. (2007). DNA binding and antimicrobial studies of some polyethyleneimine-copper(II) complex samples containing 1,10-phenanthroline and l-theronine as co-ligands. *Polyhedron*, 26(13), 3255–3262. doi:10.1016/j.poly.2007.03.001
- Liang, J.-X., Zhong, H.-J., Yang, G., Vellaisamy, K., Ma, D.-L., & Leung, C.-H. (2017). Recent development of transition metal complexes with in vivo antitumor activity. *Journal of Inorganic Biochemistry*, 177, 276–286. doi:10.1016/j.jinorgbio.2017.06.002
- Liu, M., Yuan, W.-B., Zhang, Q., Yan, L., & Yang, R.-D. (2008). Synthesis, characterization and DNA interaction studies of complexes of lanthanide nitrates with tris {2-[(3,4-dihydroxybenzylidene) imino]ethyl} amine. *Spectrochimica Acta Part A: Molecular and Biomolecular Spectroscopy*, 70(5), 1114–1119. doi:10.1016/j.saa.2007.10.023
- Loganathan, R., Ramakrishnan, S., Suresh, E., Riyasdeen, A., Akbarsha, M. A., & Palaniandavar, M. (2012). Mixed ligand copper(II) complexes of N,N-bis(benzimidazol-2-ylmethyl) amine (BBA) with diimine co-ligands: Efficient chemical nuclease and protease activities and cytotoxicity. *Inorganic Chemistry*, 51(10), 5512–5532. doi:10.1021/ic2017177
- Luo, Z., Shi, X., Hu, Q., Zhao, B., & Huang, M. (2012). Structural evidence of perfluorooctane sulfonate transport by human serum albumin. *Chemical Research in Toxicology*, 25(5), 990–992. doi:10.1021/tx300112p
- Mahamoud, A., Chevalier, J., Davin-Regli, A., Barbe, J., & Pages, J.-M. (2006). Quinoline derivatives as promising inhibitors of antibiotic efflux pump in multidrug resistant Enterobacter aerogenes isolates. *Current Drug Targets*, 7(7), 843–847. doi:10.2174/13894500677709557
- Mansouri-Torshizi, H., Moghaddam, M., Divsalar, A., & Saboury, A. (2009). Diimine platinum(II) and palladium(II) complexes of dithiocarbamate derivative as potential antitumor agents: Synthesis, characterization, cytotoxicity, and detail DNA-binding studies. *Journal of Biomolecular Structure and Dynamics*, 26(5), 575–586. doi:10.1080/07391102.2009.10507273
- Mansouri-Torshizi, H., Rezaei, E., Kamranfar, F., & Majd, M. H. (2016). Investigating the apoptosis ability of ethylenediamine 8-hydroxyquinolinato palladium(II) complex. *Advanced Pharmaceutical Bulletin*, 6(3), 449–453. doi:10.15171/apb.2016.058
- Mansouri-Torshizi, H., Saeidifar, M., Rezaei-Behbehani, G., Divsalar, A., & Saboury, A. (2010). DNA Binding Studies and Cytotoxicity of Ethylenediamine 8-Hydroxyquinolinato Palladium(II) Chloride. *Journal of the Chinese Chemical Society*, 57(6), 1299–1308. doi:10.1002/jccs.201000192
- Messori, L., Orioli, P., Vullo, D., Alessio, E., & Iengo, E. (2000). A spectroscopic study of the reaction of NAMI, a novel ruthenium(III) anti-neoplastic complex, with bovine serum albumin. *European Journal of Biochemistry*, 267(4), 1206–1213. doi:10.1046/j.1432-1327.2000.01121.x
- Milutinović, M. M., Rilak, A., Bratsos, I., Klisurić, O., Vraneš, M., Gligorijević, N., ... Bugarić, Ž. D. (2017). New 4'-(4-chlorophenyl)-2,2':6',2''-terpyridine ruthenium(II) complexes: Synthesis, characterization, interaction with DNA/BSA and cytotoxicity studies. *Journal of Inorganic Biochemistry*, 169, 1–12. doi:10.1016/j.jinorgbio.2016.10.001
- Musiol, R., Jampilek, J., Kralova, K., Richardson, D. R., Kalinowski, D., Podeszwa, B., ... Polanski, J. (2007). Investigating biological activity spectrum for novel quinoline analogues. *Bioorganic and Medicinal Chemistry*, 15(3), 1280–1288. doi:10.1016/j.bmc.2006.11.020
- Nakamoto, K. (2008). *Infrared and Raman Spectra of Inorganic and Coordination Compounds, Theory and Applications in Inorganic Chemistry*. New York: Wiley.
- Nicholson, J., Wolmarans, M., & Park, G. (2000). The role of albumin in critical illness. *British Journal of Anaesthesia*, 85(4), 599–610.

- Olmsted III, J., & Kearns, D. R. (1977). Mechanism of ethidium bromide fluorescence enhancement on binding to nucleic acids. *Biochemistry*, 16(16), 3647–3654. doi:10.1021/bi00635a022
- Palit, P., Paira, P., Hazra, A., Banerjee, S., Gupta, A. D., Dastidar, S. G., & Mondal, N. B. (2009). Phase transfer catalyzed synthesis of bis-quinolines: antileishmanial activity in experimental visceral leishmaniasis and in vitro antibacterial evaluation. *European Journal of Medicinal Chemistry*, 44(2), 845–853. doi:10.1016/j.ejmech.2008.04.014
- Ramachandran, E., Raja, D. S., Bhuvanesh, N. S., & Natarajan, K. (2013). Synthesis, characterization and in vitro pharmacological evaluation of new water soluble Ni(II) complexes of 4N-substituted thiosemicarbazones of 2-oxo-1,2-dihydroquinoline-3-carbaldehyde. *European Journal of Medicinal Chemistry*, 64, 179–189. doi:10.1016/j.ejmech.2013.03.059
- Ray, S., Mohan, R., Singh, J. K., Samantaray, M. K., Shaikh, M. M., Panda, D., & Ghosh, P. (2007). Anticancer and antimicrobial metallodrug agents based on palladium, gold, and silver N-heterocyclic carbene complexes. *Journal of the American Chemical Society*, 129(48), 15042–15053. doi:10.1021/ja075889z
- Saeidifar, M., Mansouri-Torshizi, H., Divsalar, A., & Saboury, A. A. (2013). Novel 2,2'-bipyridine palladium(II) complexes with glycine derivatives: Synthesis, characterization, cytotoxic assays and DNA-binding studies. *Journal of the Iranian Chemical Society*, 10(5), 1001–1011. doi:10.1007/s13738-013-0237-1
- Saeidifar, M., Mansouri-Torshizi, H., Palizdar, Y., Eslami-Moghaddam, M., Divsalar, A., & Saboury, A. A. (2014). Synthesis, characterization, cytotoxicity and DNA binding studies of a novel anionic organopalladium(II) complex. *Acta Chimica Slovenica*, 61(1), 126–136.
- Saeidifar, M., Sohrabi Jam, Z., Shahraki, S., Khanlarkhani, A., Javaheri, M., Divsalar, A., ... Akbar Saboury, A. (2017). Multi-spectroscopic and electrochemical approaches of the interaction between a new binuclear agent and DNA. *Journal of Biomolecular Structure and Dynamics*, 35(12), 2557–2564. doi:10.1080/07391102.2016.1229635
- Sargazi, A., Kuhestani, K., Nosrat Nahoki, T., & Heidari Majd, M. (2015). Specific targeting of folate receptor by methotrexate conjugated modified magnetic nanoparticles: Enzymatic release and cytotoxic study. *International Journal of Pharmaceutical Sciences and Research*, 6(12), 5047–5055.
- Scatchard, G. (1949). The attractions of proteins for small molecules and ions. *Annals of the New York Academy of Sciences*, 51(4), 660–672. doi:10.1111/j.1749-6632.1949.tb27297.x
- Schwartzmann, G., Winograd, B., & Pinedo, H. (1988). The main steps in the development of anticancer agents. *Radiotherapy and Oncology*, 12(4), 301–313.
- Shahraki, S., Mansouri-Torshizi, H., Nezami, Z. S., Ghahghaei, A., Yaghoobi, F., Divsalar, A., & Shirazi, F. H. (2014). The effects of extending of co-planarity in a series of structurally relative polypyridyl Palladium (II) complexes on DNA-binding and cytotoxicity properties. *Iranian Journal of Pharmaceutical Research*, 13(4), 1279–1294.
- Shahraki, S., Shiri, F., Majd, M. H., & Razmara, Z. (2017). Comparative study on the anticancer activities and binding properties of a hetero metal binuclear complex $[\text{Co}(\text{dipic})_2 \text{Ni}(\text{OH})_2] \cdot 5 \cdot 2\text{H}_2\text{O}$ (dipic = dipicolinate) with two carrier proteins. *Journal of Pharmaceutical and Biomedical Analysis*, 145, 273–282. doi:10.1016/j.jpba.2017.06.067
- Shahraki, S., Shiri, F., & Saeidifar, M. (2018). Synthesis, characterization, in silico ADMET prediction, and protein binding analysis of a novel zinc(II) Schiff-base complex: Application of multi-spectroscopic and computational techniques. *Journal of Biomolecular Structure and Dynamics*, 36(7), 1666–1680. doi:10.1080/07391102.2017.1334595
- Shi, J.-H., Lou, Y.-Y., Zhou, K.-L., & Pan, D.-Q. (2018). Probing the behavior of calf thymus DNA upon binding to a carboxamide fungicide boscalid: Insights from spectroscopic and molecular docking approaches. *Journal of Biomolecular Structure and Dynamics*, 36(10), 2738–2745. doi:10.1080/07391102.2017.1365012
- Shiri, F., Shahraki, S., Baneshi, S., Nejati-Yazdinejad, M., & Majd, M. H. (2016). Synthesis, characterization, in vitro cytotoxicity, in silico ADMET analysis and interaction studies of 5-dithiocarbamate-1,3,4-thiadiazole-2-thiol and its zinc(II) complex with human serum albumin: Combined spectroscopy and molecular docking investigations. *RSC Advances*, 6(108), 106516–106526. doi:10.1039/C6RA17322E
- Shiri, F., Shahraki, S., Shahriyar, A., & Majd, M. H. (2017). Exploring isoxsuprine hydrochloride binding with human serum albumin in the presence of folic acid and ascorbic acid using multispectroscopic and molecular modeling methods. *Journal of Photochemistry and Photobiology B: Biology*, 170, 152–163. doi:10.1016/j.jphotobiol.2017.04.007
- Shiri, F., Shahraki, S., & Shahriari, S. (2018). Mechanistic understanding and binding analysis of a novel Schiff base palladium (II) complex with β -lactoglobulin and human serum albumin. *Journal of Molecular Liquids*, 262, 218–229. doi:10.1016/j.molliq.2018.04.078
- Sorinezami, Z., & Mansouri-Torshizi, H. (2016). Photo-catalytic degradation of organic dyes: Ultrasonic-assisted synthesis of PdO nanoparticles. *Journal of Materials Science: Materials in Electronics*, 27(2), 1558–1565. doi:10.1007/s10854-015-3924-0
- Sorinezami, Z., Mansouri-Torshizi, H., & Ghanbari, B. (2017). Synthesis of PdO nanoparticles: Crystal structure, DNA binding, and cytotoxicity of a new hydroxyl-quinolinato-palladium complex. *Inorganic and Nano-Metal Chemistry*, 47(4), 500–508. doi:10.1080/15533174.2016.1186079
- Sun, Y.-G., Sun, Y.-N., You, L.-X., Liu, Y.-N., Ding, F., Ren, B.-y., ... Dragutan, I. (2016). Novel mononuclear Pt^{2+} and Pd^{2+} complexes containing (2,3-f)pyrazino (1,10)phenanthroline-2,3-dicarboxylic acid as a multi-donor ligand. Synthesis, structure, interaction with DNA, in vitro cytotoxicity, and apoptosis. *Journal of Inorganic Biochemistry*, 164, 129–140. doi:10.1016/j.jinorgbio.2016.09.008
- Tarushi, A., Kakoulidou, C., Raptopoulou, C. P., Psycharis, V., Kessissoglou, D. P., Zoi, I., ... Psomas, G. (2017). Zinc complexes of diflunilal: Synthesis, characterization, structure, antioxidant activity, and in vitro and in silico study of the interaction with DNA and albumins. *Journal of Inorganic Biochemistry*, 170, 85–97. doi:10.1016/j.jinorgbio.2017.02.010
- Tomás-Mendivil, E., Díez, J., & Cadierno, V. (2013). Palladium (II) complexes with symmetrical dihydroxy-2,2'-bipyridine ligands: Exploring their inter- and intramolecular interactions in solid-state. *Polyhedron*, 59, 69–75. doi:10.1016/j.poly.2013.04.043
- Ulukaya, E., Ari, F., Dimas, K., Ikitimur, E. I., Guney, E., & Yilmaz, V. T. (2011). Anti-cancer activity of a novel palladium(II) complex on human breast cancer cells in vitro and in vivo. *European Journal of Medicinal Chemistry*, 46(10), 4957–4963. doi:10.1016/j.ejmech.2011.07.055
- Ulukaya, E., Frame, F. M., Cevatemre, B., Pellacani, D., Walker, H., Mann, V. M., & Maitland, N. J. (2013). Differential cytotoxic activity of a novel palladium-based compound on prostate cell lines, primary prostate epithelial cells and prostate stem cells. *PLoS One*, 8(5), 1–13. doi:10.1371/journal.pone.0064278
- Wang, X., Herting, G., Wallinder, I. O., & Blomberg, E. (2015). Adsorption of bovine serum albumin on silver surfaces enhances the release of silver at pH neutral conditions. *Physical Chemistry Chemical Physics*, 17(28), 18524–18534. doi:10.1039/C5CP02306H
- Wang, Y., Wang, X., Wang, J., Zhao, Y., He, W., & Guo, Z. (2011). Noncovalent interactions between a trinuclear monofunctional platinum complex and human serum albumin. *Inorganic Chemistry*, 50(24), 12661–12668. doi:10.1021/ic201712e
- Yang, S.-J., Liu, M.-C., Xiang, H.-M., Zhao, Q., Xue, W., & Yang, S. (2015). Synthesis and in vitro antitumor evaluation of betulin acid ester derivatives as novel apoptosis inducers. *European Journal of Medicinal Chemistry*, 102, 249–255. doi:10.1016/j.ejmech.2015.08.004
- Zhang, G., Ma, Y., Wang, L., Zhang, Y., & Zhou, J. (2012). Multispectroscopic studies on the interaction of maltol, a food additive, with bovine serum albumin. *Food Chemistry*, 133(2), 264–270. doi:10.1016/j.foodchem.2012.01.014